Journal of Statistical Physics, Vol. 68, Nos. 1/2, 1992

Microwave Experiments on Chaotic Billiards

S. Sridhar,[1] D. O. Hogenboom,[1] and Balam A. Willemsen,[1]

Received January 22, 1992

We describe experiments using billiard-shaped microwave cavities, to test ideas in quantum chaos. The experimental method for observing cavity resonances to obtain the eigenvalues, and the advantages and limitations of the techniques, including the influence of absorption, are discussed. An experimental technique to obtain a 2D mapping of the wavefunction is described. Results are displayed for 36 of the low-lying wavefunctions of a Sinai billiard cavity consisting of a central disc in a rectangular enclosure. The wavefunctions demonstrate the influence of classical periodic orbits (PO), of which there are two types: non-isolated PO, which avoid the central disc, and isolated PO, which hit the central disc. Scarred states, including those associated with isolated PO, are directly observed.

KEY WORDS: Quantum chaos; microwave cavities; sinai billiard; eigenfunctions; eigenvalues; scarred states; periodic orbits.

While significant progress has been achieved on theoretical aspects[1] of the quantum or wave mechanics of classically chaotic systems, experimental work has gathered momentum only recently.[2] This is because the proper experimental systems, and the observable signatures of quantum chaos in particular experiments, need to be identified. While phenomena at the atomic or subatomic level are obvious experimental candidates, the common wave nature of electromagnetics and quantum mechanics suggests a new approach to experiments designed to test observable consequences of the wave aspects of classical chaos.

The correspondence between quantum mechanical problems and electromagnetic situations has long been recognized. In two dimensions, and for stationary time-independent situations, both the Maxwell and the Schrödinger equations reduce to the scalar Helmholtz equation:

[1] Department of Physics, Northeastern University, Boston, Massachusetts 02115.

0022-4715/92/0700-0239$06.50/0

$(\nabla^2 + k^2)\{E_z \text{ or } \psi\} = 0$. For bound states in closed systems and scattering states in open systems, the correspondence can be exploited to yield information on both electromagnetic and quantum mechanical situations.

This paper discusses the basis and results of recent experiments carried out in our laboratory, which exploit this correspondence, to study issues in quantum chaos. The experiments utilize microwave cavities shaped in the form of a Sinai billiard cavity. We discuss the experimental method employed to determine the eigenvalues of such cavities, and also a novel technique to obtain maps of the corresponding eigenfunctions (Section 2). The experimental features, and advantages and limitations, are described. The influence of absorption at the walls on the results is discussed (Section 3). We present some results for the eigenvalues (Section 4), and display several of the low-lying eigenfunctions of the Sinai billiard cavity (Section 5). The principal result which emerges is the connection to classical periodic orbits, and the direct observation of scars[3, 4] in the wavefunctions.

1. MICROWAVE CAVITIES

An ideal microwave cavity is a singly or multiply connected 3-dimensional domain $\mathscr{D}$ bounded by infinitely conducting walls (later we examine the effects of finite conductivity). In this domain, stationary solutions of electromagnetic waves obey the wave equation

$$(\nabla^2 + \omega^2/c^2)\{\mathbf{E}, \mathbf{B}\} = 0 \tag{1}$$

with boundary conditions requiring that $\mathbf{E}$ normal to $\mathscr{D}$ and $\mathbf{B}$ tangential to $\mathscr{D}$ vanish.

If the cavity is cylindrical, i.e., is uniform in the z direction, but has arbitrary cross section, then the fields can be expressed as

$$\mathbf{E}\{\mathbf{B}\} = \mathbf{E}\{\mathbf{B}\}(x, y)\exp(ik_z z - i\omega t) \tag{2}$$

Substituting, we get

$$[\nabla_t^2 + (k^2 - k_z^2)]\{\mathbf{E}, \mathbf{B}\} = 0 \tag{3}$$

where $\nabla_t^2 = \nabla^2 - \partial^2/\partial z^2$ and $k = \omega/c$.

The fields can be expressed in terms of transverse (t) and axial (z) components, viz. $\mathbf{E}\{\mathbf{B}\} = \mathbf{E}_z\{\mathbf{B}_z\} + \mathbf{E}_t\{\mathbf{B}_t\}$. It is then possible to show that the transverse components $\mathbf{E}_t$ and $\mathbf{B}_t$ can be calculated in terms of the z components $\mathbf{E}_z$ and $\mathbf{B}_z$ only:

$$\mathbf{E}_t\{\mathbf{B}_t\} = \frac{1}{k^2 - k_z^2}\left[\nabla_t\left(\frac{\partial E_z\{B_z\}}{\partial z}\right) + \{-\}ik\hat{z}\times\nabla_t B_z\{E_z\}\right] \tag{4}$$

If the cavity has a thickness d along the z direction, then the boundary conditions require that $k_z = p\pi/d$. Equation (3) can then be written as

$$[\nabla_t^2 + (k^2 - (p\pi/d)^2]\{E_z, B_z\} = 0 \tag{5}$$

Two classes of modes are possible:

TE (Transverse Electric) Modes: $E_z = 0$ everywhere.

Since B_z must vanish at $z = 0$ and d, the only solutions allowed are of the form $B_z = B_z(x, y)\sin(p\pi z/d)$, which requires that $p \neq 0$. Thus, all the TE modes must have a variation along z, and hence can never be treated as 2-dimensional. We ignore these modes in the subsequent discussion.

TM (Transverse Magnetic) Modes: $B_z = 0$ everywhere.

From Eq. (4) the allowed solutions are $E_z = E_z(x, y)\cos(p\pi z/d)$, so that E_z is nonzero at $z = 0$ and $z = d$. Here $p = 0$ is allowed and hence there is a class of TM modes which have no variation along the z direction, and hence are 2-dimensional. We confine our subsequent discussion to these modes only. Below we summarize the properties of these states:

2-Dimensional Transverse Magnetic Modes ($p = 0$):

$$[\nabla_t^2 + k^2]E_z = 0 \tag{6}$$

$$E_z = E_z(x, y) \tag{7}$$

$$\mathbf{B}_t = (i\omega/c\gamma^2)\hat{z} \times \nabla_t E_z \tag{8}$$

$$B_z = 0, \qquad E_t = 0 \text{ everywhere} \tag{9}$$

It is useful to recall the solutions for the case of a rectangle of dimensions $a \times b$. Here the eigenvalues are given by $\omega^2 = c^2[(n\pi/a)^2 + (m\pi/b)^2]$, and the eigenfunctions by

$$E_z = E_0 \sin(n\pi x/a)\sin(m\pi y/b)$$

$$B_x \propto \sin(n\pi x/a)\cos(m\pi y/b)$$

$$B_y \propto \cos(n\pi x/a)\sin(m\pi y/b)$$

In general, for arbitrary cross section, all modes which have an eigenfrequency $\omega < c\pi/d$ are guaranteed to be 2-dimensional. The number of modes which satisfy this criterion will be determined by the relative values of d and the (x, y) dimensions. This is important from an experimental point of view, since then these modes are easy to identify as being all the ones below a maximum frequency. Of course 2D modes will occur at all frequencies, but will be interspersed among $p \neq 0$ modes.

For completeness, we state the correspondence between the EM and the QM situations. For the eigenvalues, $k^2 = \omega^2/c^2 \Leftrightarrow E = \hbar^2 k^2/2m$. The

classical limit of the QM problem is obtained when the de Broglie wavelength $\lambda = \hbar/k \ll$ dimensions of $\mathscr{D}$. This is equivalent to the geometrical optics or ray limit of the EM problem, where the wavelength $\lambda = c/f \ll$ dimensions of $\mathscr{D}$.

2. EXPERIMENTAL TECHNIQUES

For the closed systems studied in this work, the principal quantities of interest are the eigenvalues and the eigenfunctions of the bound states. This section discusses the experimental observation of these quantities.

The geometries studied in this work were a Sinai billiard consisting of a rectangle with a circular disc inside, and a bare rectangle [Fig. 1 (top)]. The cavities consist of top and bottom plates, and side bars of thickness 6 mm all tightly bolted together. The circular disc, also of thickness 6 mm, could be placed anywhere in the rectangular enclosure. All material was made of OFHC copper polished to a high finish.

2.1. Measuring Eigenvalue Resonances

Microwaves were coupled into and out of a cavity via coax probes terminated by loops connected to the center and outer conductors of the coax. The coupling ports of diameter .085 in. through which the coax were inserted were located on the side bars at half the cavity height [Fig. 1

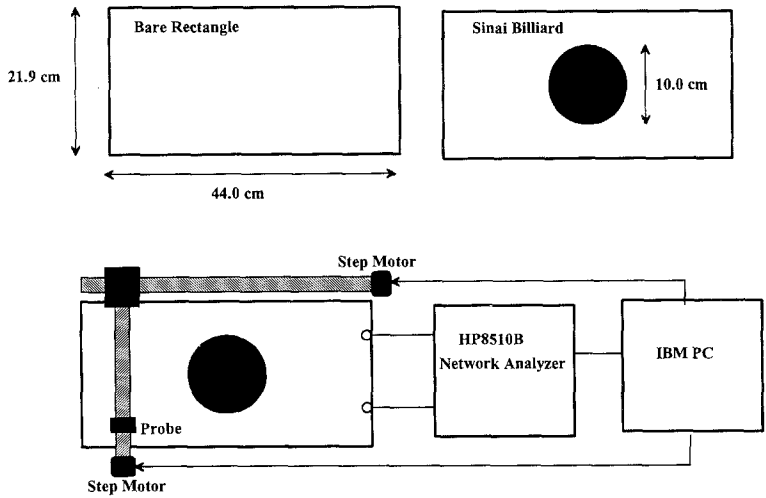

Fig. 1. (Top) The two cavity geometries studied: a rectangle and a Sinai billiard. (Bottom) Schematic diagram of the experimental setup showing the Sinai billiard cavity, the mechanism for positioning the perturbing ball, and the microwave analyzer.

(bottom)]. This method couples dominantly to the transverse B fields on the sides. It is important to note that the coupling could be varied by orders of magnitude by inserting or withdrawing the coax, and also by orienting the loop. All the measurements reported here were carried out using the weakest coupling allowable. The experimental technique is similar to those used extensively[5] in this laboratory to study both normal (Cu) cavities and superconducting (high T_c, Nb and Pb) cavities, with Q's ranging from 10^3 to 10^9.

The cavities were studied in a transmission mode [Fig. 1 (bottom)], using an HP8510B Network Analyzer (ANA), driven by a HP8431B synthesizer capable of providing signals between 45 MHz and 20 GHz. The ANA enables one to study the transmission function $S_{21}(f)$ of the cavities over any chosen bandwidth at $f < 20$ GHz. Although both amplitude and phase are measurable, only the amplitude is important here.

A typical transmission trace $S_{21}(f)$ vs. frequency $f = \omega/2\pi$ between 3.1 and 3.5 GHz is shown in Fig. 2 for the Sinai billiard cavity. Several resonance peaks are clearly identifiable. As expected, the transmission function for each resonance appears to be Lorentzian. However, the trace also illustrates a limitation of the experiment. Because of the finite width, very closely spaced resonances may overlap. By substantial frequency magnification, it is possible to distinguish between overlapping resonances —sometimes they appear as shoulders on larger peaks, or as distinct but overlapping peaks. With care, and some judgment, it is possible to identify all eigenfrequencies except those which overlap within about 1/10 of the resonance width. Thus, slightly broken degeneracies and accidental near degeneracies may be missed.

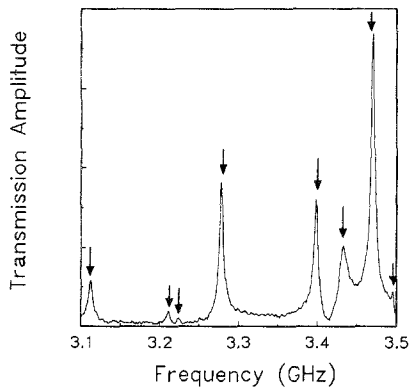

Fig. 2. Typical transmission amplitude vs. frequency plot showing several resonance peaks (eigenfrequencies) for the Sinai billiard.

The finite width of the resonances is due to absorption in the walls. We discuss the role of absorption and the influence of overlapping resonances on the spacing statistics in appropriate sections later.

It is well known that in this method of measuring cavity properties, each cavity eigenmode can be regarded as a driven, damped, harmonic oscillator. The coupling mechanism, which acts as a weak perturbation, can modify the cavity properties in two ways: frequency-pulling, i.e., shift of resonance frequency, and loading, i.e., reduction of Q. However, the actual parameter values used were such that both these effects of the coupling were negligible in comparison to the major contributions to non-ideality, viz. absorption in the walls and slight geometric imperfections of the cavity. *Thus, the means of observation of the cavity were the weakest perturbations in our experiments.*

2.2. Mapping Eigenfunctions

While the eigenfrequencies are easily observed, obtaining a full 2D mapping of the eigenfunctions poses special challenges. A natural method may appear to be to have another coupling port in the top or bottom plates and to insert a measuring probe. If the port + probe could be moved, then in principle one could measure the field amplitudes at various positions. This obvious method was not attempted, as it is quite cumbersome.

Instead we use a technique that utilizes a cavity perturbation method, in which the frequency shift caused by a metallic object placed inside the cavity is a measure of the local field at the object location. For a metallic object, the frequency shift of the resonance from its unperturbed value f_0 is given by[6]

$$\frac{\Delta f}{f_0} = -\frac{\int (\alpha E^2 - \beta B^2)\, dV_b}{U} \tag{10}$$

where α and β are geometric factors determined by the shape, the integration is over the sample (bead) volume, and U is the energy density in the cavity. For a very small, needlelike bead with the long axis parallel to the E field, the above equation can be written as

$$\Delta f(x, y) = -kE_z^2(x, y) \qquad \text{or} \qquad E_z^2(x, y) = -\Delta f(x, y)/k \tag{11}$$

where k is a geometric factor independent of position. Thus $E_z^2(x, y)$ can be measured, to within a scale factor, by moving a metallic bead over the cross section of the cavity.

2.2.1. 1D Wavefunction Slices. In our *initial* experiments, we employed a metallic bead attached to a nylon fishing line. By pulling the line using a stepper motor and measuring the resonance peak of a particular eigenmode transmission resonance as the bead was stepped from one end to another using about 200 steps, we were able to obtain a 1D slice of the wavefunction. The result for the 10.78-GHz mode of the rectangular cavity is shown in Fig. 3 (top), along with the direction of the bead motion, which is displayed in the inset. The periodic nature is apparent, and the data follow the expected sine-squared behavior.

Similar results for the 16.27-GHz mode of the Sinai billiard cavity are shown in Fig. 3 (bottom). The aperiodic nature of the wavefunction is clearly obvious, and was (for us at least) the first evidence of unusual wavefunctions in the billiard cavity, and provided encouraging results for further studies.

The above method is often used in studying accelerator structures. However, a little reflection shows that 1D slices are clearly inadequate, and results depend crucially on the particular slice chosen. Thus, a 2D method was necessary. This was particularly challenging, since, to our knowledge, wavefunctions had not been measured in more than one dimension.

2.2.2. Measuring Wavefunctions in 2D. A 2D implementation of the cavity perturbation technique was carried out by employing a steel magnetic bead which could be "dragged" along the top surface of the cavity

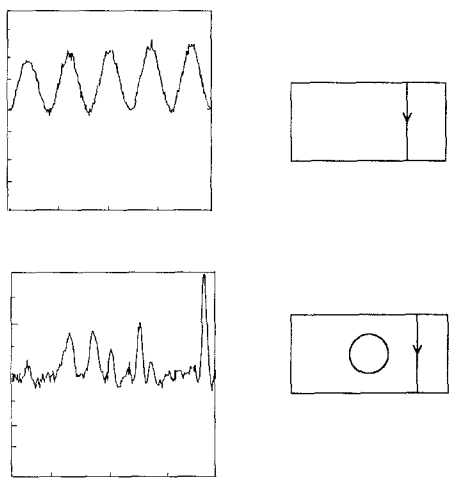

Fig. 3. Experimentally measured one-dimensional "slice" of E_z^2 for (top) the 10.78-GHz mode of the rectangular cavity, and (bottom) the 16.27-GHz mode of the Sinai billiard cavity. The trajectory of the "slice" for each case is shown on the right.

by external magnetic means. Typically the bead is moved to locations on a grid and the resonance frequency is measured for each grid location. Taking the unshifted resonance frequency to be when the bead is at a corner, the frequency shifts for each grid location are obtained. These frequency shifts then yield E_z^2 by using Eq. (11). The data are typically converted to contour plots, although we have also found other representations, such as density plots, to be also informative. This is repeated for each resonance, and thus the eigenfunction corresponding to each eigenvalue is then obtained. The speed of acquiring the wavefunctions is primarily limited by the mechanical motion and by the need to noise-average transmission traces for small resonance peaks. For low frequencies and coarse grids ($\sim$0.5–1 cm) typical wavefunction acquisition time is about 20 min.

Several precautions are needed in order to acquire accurate data. Adequate resolution is easily ensured by using appropriately small grid step sizes, which need to be less than $\lambda/10$ to $\lambda/5$, where $\lambda = c/f$ is the free-space wavelength. It is most important to ensure that the perturbation due to the bead does not itself affect the measurement. This perturbation would principally lead to a mixing of states, particularly neighboring ones. This is prevented by choosing an appropriately small bead, using a rule of thumb that the maximum frequency shift is much smaller, say 1/5 of the resonance width. This also ensures that the maximum frequency shift is very small compared to the nearest neighbor spacing for well-separated resonances. The problem arises for resonances which are not well separated, particularly for ones that appear as shoulders of larger resonances. Occasionally these wavefunctions cannot be measured. Finally, since the bead perturbation represented by the geometric factor k in Eq. (11) increases linearly with f and bead volume V_b, smaller beads are required for higher frequencies. With these precautions, it is possible to observe reliably the eigenfunctions for all but a small fraction of the observed eigenvalues, as the subsequent discussion in Section 5 shows.

While the major perturbation caused by the bead is due to the E field, there is a small contribution due to the B field for the spherical metallic object used here. This is evident from the observation of a small, positive frequency shift where the E field is known to be zero. Thus, a more exact representation of the bead perturbation is $\Delta f = -k_E E_z^2 + k_B B_t^2$. In practice, the B-field contribution is small (estimated to be about a few percent), and is eliminated by ignoring all positive frequency shifts.

3. EFFECTS OF FINITE ABSORPTION (i.e., Q)

A fundamental premise of the relation of the experimental work to theoretical considerations is that the influence of absorption, which is

always present in an experiment, is minimal and even ignorable. Here we examine this premise and consider the specific effects of absorption.

Absorption arises in real cavities due to the presence of walls which have a finite conductivity, or equivalently a finite skin depth. This has two direct consequences: (1) a small shift of the resonance frequency, and (2) a broadening of each resonance.

The resonance frequency shift can be understood as if the dimensions of the cavity were extended by one skin depth. This is because in a real metal, the tangential E and normal B fields do not terminate at the physical boundary, but extend approximately one skin depth into the metal. For Cu at room temperature, the skin depth varies as $\delta_{\mathrm{Cu}} = 2.075/\sqrt{f}$ (μm), where f is in GHz. Thus, the skin depth varies from about 2 μm to 0.5 μm between 1 and 20 GHz. The corresponding resonance frequency shifts can be estimated as $\Delta f_0/f_0 \sim \delta_{\mathrm{Cu}}/a$, where a [$\sim O(10^2\,\mathrm{cm})$] is the (approximate) linear dimension in the xy plane. Thus, the shift of the resonances from their ideal location f_0 due to absorption is about $10^{-5} f_0$, i.e., about 100 kHz in the frequency range of measurement. This is negligible, since the accuracy of the dimensions is about 10^{-4} at best.

On the other hand, the broadening of the resonances has important consequences, principally leading to eigenvalues which may be missed due to overlapping neighboring resonances (see Section 4). In order to understand this quantitatively, it is useful to use the notion of the Q of the cavity, which is defined in terms of the resonance half-width as $Q = f_0/\delta f$, and which is typically 10^4. Consider the TM modes of a rectangular cavity of dimensions $a \times b \times d$. Then

$$\frac{Q_{\mathrm{TM}}}{f_{mn0}} = \frac{\mu \sigma_{\mathrm{Cu}} \delta_{\mathrm{Cu}} \pi d (m^2 b^2 + n^2 a^2)\, ab}{ab(m^2 b^2 + n^2 a^2) + 2d(n^2 a^3 + m^2 b^3)} \tag{12}$$

where m, n define the mode. If $d \ll a, b$ as is the case here, then $Q \approx (\mu_0 \sigma_{\mathrm{Cu}} \delta_{\mathrm{Cu}} \pi d) f \propto \sqrt{f}$, since $\delta_{\mathrm{Cu}} \propto 1/\sqrt{f}$. Thus, the resonance width $\delta f \propto \sqrt{f}$, i.e., the resonance width, and hence the problem of overlapping resonances, increases with frequency.

For a general cavity, including the Sinai billiard, the Q of a mode can always be expressed as $Q = \Gamma/R_s$, where R_s is the surface resistance ($\propto \sqrt{f}$ for a normal metal), and Γ is a geometric factor and is mode specific. At high frequency, $\Gamma \propto f$. Thus, in all cavities made of normal metal, $Q \propto \sqrt{f}$. (This has been shown experimentally,[5] and also that for superconducting cavities $Q \propto 1/f$, since $R_s \propto f^2$. The use of superconducting cavities would remove the present limitations due to absorption, since the Q's would be at least 10^3–10^4 times higher due to very low R_s.)

In practice it is possible to distinguish resonances which are spaced

greater than about 1/10 of the resonance width. The principal consequence of missing eigenvalues is in the spacing statistics, as discussed later.

The finite absorption does not affect the eigenfunctions of well-spaced resonances, as is apparent from later sections. However, the resonance width does lead to mixed states, and limits the observation of pure states when neighboring resonances overlap.

4. RESULTS FOR THE EIGENVALUES

Using the procedure outlined in Section 2, we have determined all the eigenfrequencies which could be definitely identified below 20 GHz. For the bare rectangle, about 820 eigenfrequencies were obtained, while for the Sinai billiard, about 780 were obtained. We discuss below some preliminary results of analysis of these data.

One of the important theoretical results in quantum chaos has been the recognition of different universality classes for the eigenvalue spacing statistics in regular and chaotic systems. In Figs. 4 (top) and 4 (bottom) we

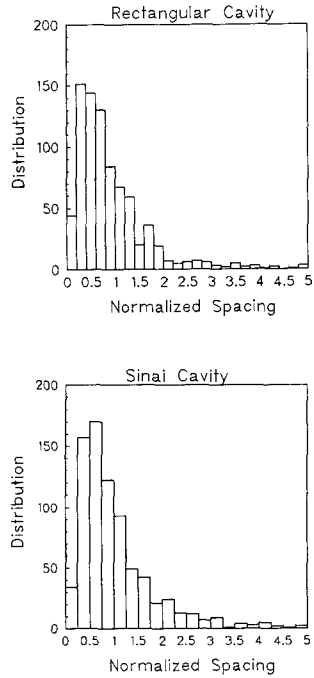

Fig. 4. Raw spacing statistics for (top) the rectangular cavity, and (bottom) the Sinai billiard cavity.

plot the *raw* spacing statistics of the eigenvalues of the rectangle and Sinai billiard in terms of the number of eigenvalues vs. the normalized spacing of the observed levels. (A much more detailed study of the spacing statistics obtained by unfolding the spectrum will be presented elsewhere. Here we only discuss the important features and the advantages and limitations of the experimental method.) The normalized spacing was simply obtained from the actual nearest neighbor spacing by normalizing to the mean spacing calculated from all the observed levels.

The most obvious feature of the data in Fig. 4 is the similarity between the spacing statistics of both the integrable (rectangular) cavity and the chaotic (Sinai billiard) cavity. This, of course, is not what is expected on theoretical grounds, since the rectangle should obey Poisson statistics, $P(s) \propto \exp(-s)$, and the Sinai billiard should obey GOE or Wigner statistics, $P(s) \propto s \exp(-\pi s^2/4)$. Although the Sinai billiard spacing statistics appears to be Wigner-like, so does the spacing statistics for the rectangle! The obvious discrepancy is in the rectangle case, where the data do not continue to increase as $s \to 0$. We believe that the reason for this is that closely spaced resonances are missed due to the resonance width caused by the absorption. This is most severe when $s \to 0$, and hence suppresses the expected Poisson behavior in the case of the rectangle. The particular aspect ratio of nearly 2:1 for the rectangle leads to many degenerate levels, which of course would not be measured in the experiment. We are currently carrying out a more detailed study of the spacing statistics, and a much more comprehensive analysis of both $P(s)$ and other statistical measures will be published elsewhere.

5. RESULTS FOR THE EIGENFUNCTIONS

The cavity experiments here are particularly powerful[4] for studying eigenfunctions, as the following discussion shows.

5.1. Rectangular (Integrable) Cavity

We first illustrate the results by displaying some eigenfunctions of the bare rectangular cavity (Fig. 5). In this and all other plots, the positive frequency shifts, associated with a B^2 term as discussed in Section 2, have been subtracted from the data. The mode structure is clearly identifiable, and the mode quantum numbers are easily obtainable. Thus, the two eigenfunctions shown in Fig. 5 have quantum numbers (2, 8) and (1, 13). The eigenfrequencies can be directly calculated since the quantum numbers are known, and are 3.053 and 4.482 GHz, which are in agreement with the

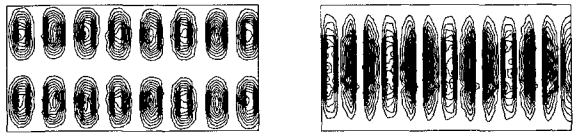

Fig. 5. Experimental contour plots of two wavefunctions of the rectangular cavity.

measured values 3.053 and 4.483 GHz to within 0.1%. The wavefunction clearly has the expected $\sin^2(n\pi x/a)\sin^2(m\pi/b)$ behavior. We have studied many more eigenfunctions of the bare rectangle. In each case the results are unambiguous, and exactly as expected.

The control experiments with the rectangle are important in providing reassurance of the following points. Once the quantum numbers are identified, experiment and theory agree to better than 0.1%. It is also clear that the structure of the eigenfunctions is not affected by the absorption in the walls or geometric imperfections. Last, but not the least, is the conclusion that the measurement technique, i.e., the perturbations introduced by the coupling ports and the measuring bead, can be controlled so as to be essentially ignorable. *We conclude that the measurement method does not introduce chaos into the integrable system.*[7]

5.2. Sinai Billiard Cavity

The wavefunctions of the Sinai billiard cavity display a rich and fascinating variety of patterns, as shown in Fig. 6, in contrast to the known results for the integrable, rectangular cavity. Shown in Fig. 6 are 36 of the lowest-lying eigenfunctions. We have carried out measurements of the eigenfunctions up to at least 10 GHz, corresponding to level numbers of several hundred. The displayed wavefunctions are illustrative of the features that are observed at higher frequencies, although of course the latter are more complex.

Not all of the lowest-lying eigenfunctions are displayed in Fig. 6. The wavefunctions corresponding to resonances peaks observed at 1.571, 1.788, 1.801, 3.829, 4.224, 4.327, and 4.449 GHz were not measurable due to weak coupling or strong overlap. Also, the particular geometry chosen has accidental near-degeneracies of eigenstates that are either even or odd with respect to reflections about the central vertical axis. These levels, although distinct in principle, are split by amounts much less than the individual resonance widths. For instance, the ground state, which is even–even, should have a partner which is odd–even and which has a node along the vertical axis.

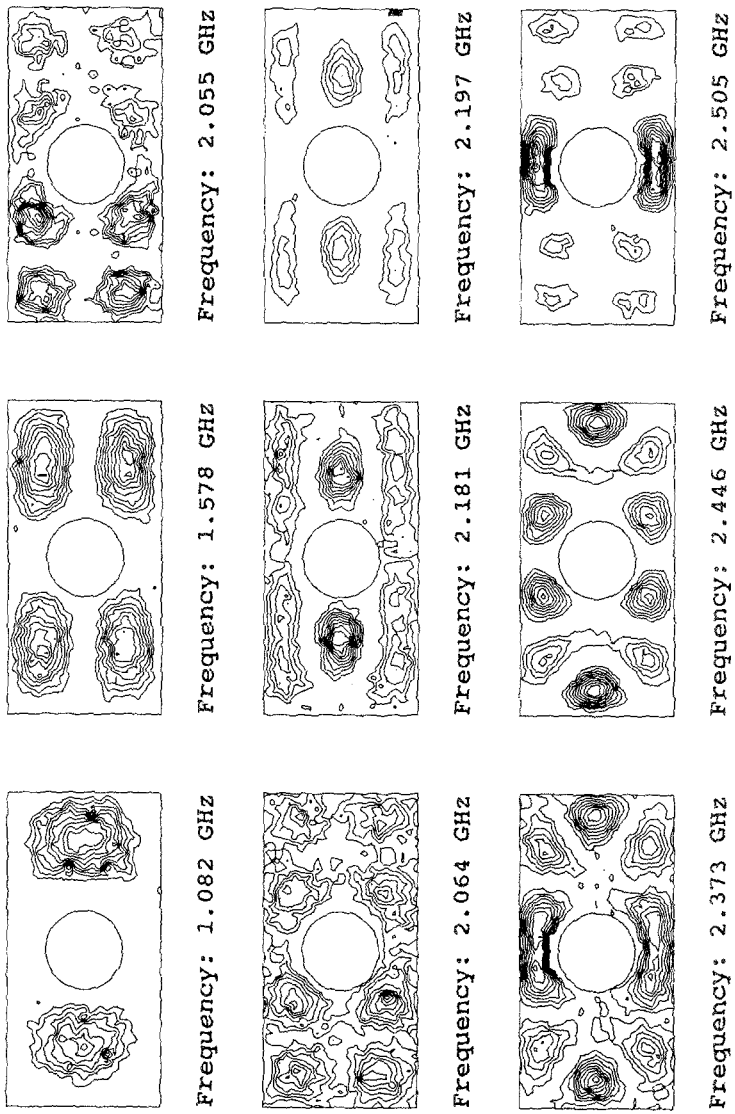

Fig. 6. Experimental contour plots of the wavefunctions of low-lying eigenstates of the Sinai billiard.

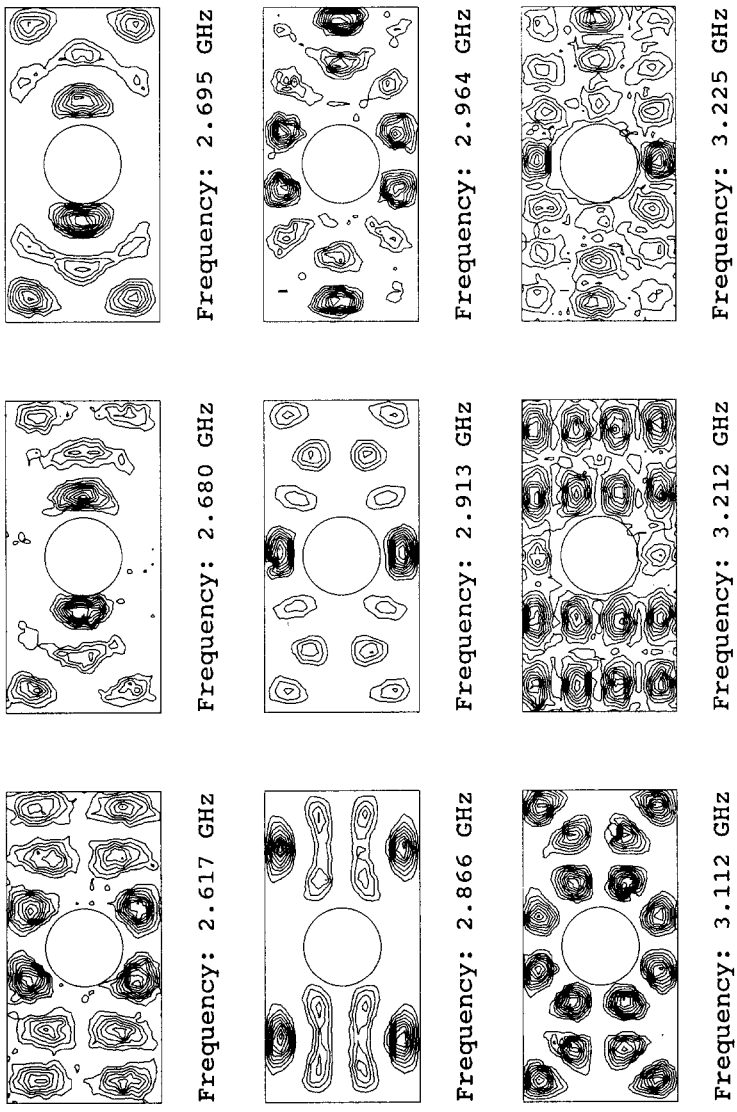

Fig. 6. (*Continued*)

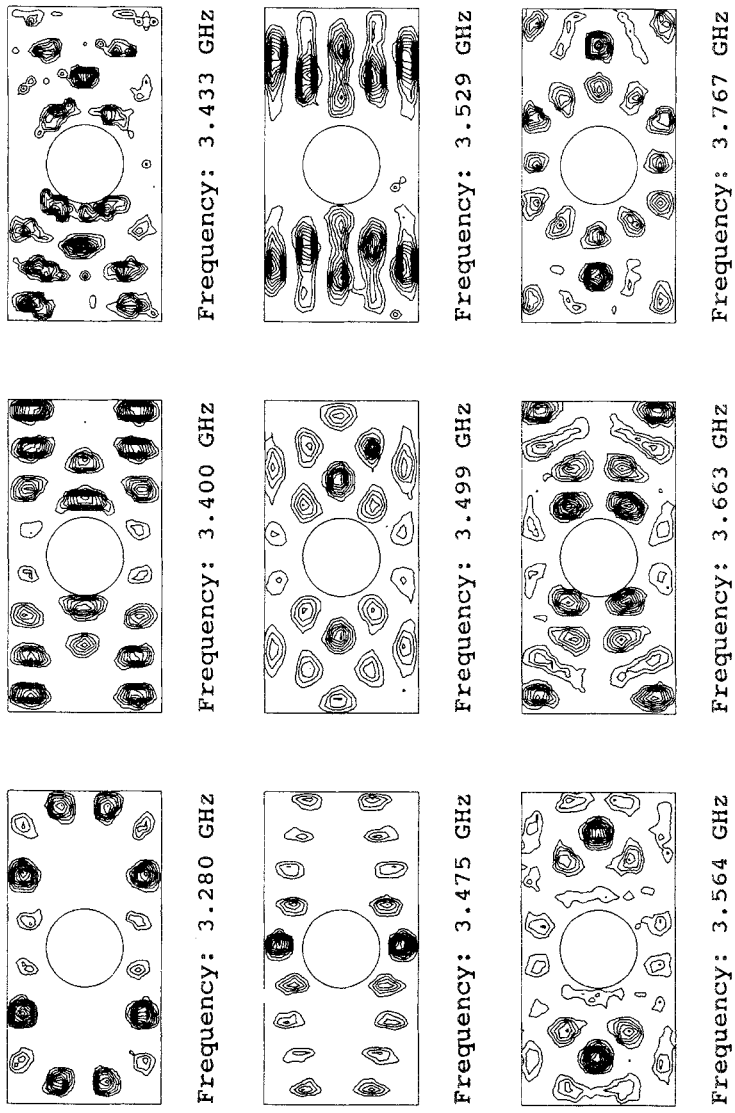

Fig. 6. *(Continued)*

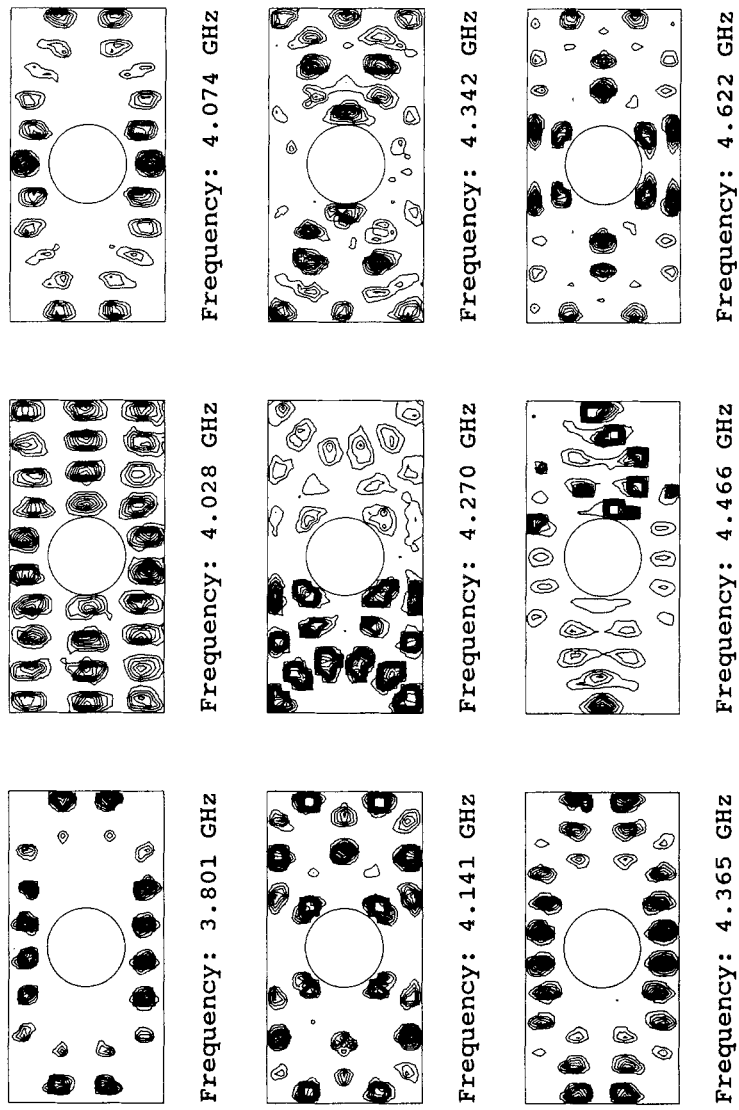

Fig. 6. (*Continued*)

A striking difference between the wavefunctions presented for the integrable rectangle system in Fig. 5 and the chaotic system in Fig. 6 is that, in the case of the integrable system (Fig. 5), the quantum numbers (i.e., for k_x and k_y) associated with each eigenfunction are immediately obtained. Furthermore, knowledge of the quantum numbers yields the corresponding eigenvalue, using analytical formulas. In contrast, for the chaotic billiard, these quantum numbers do not exist. This is evident from the wavefunctions displayed in Fig. 6. Since there are no exact rules of quantization, an exact connection between the eigenfunction and the corresponding eigenvalue is not possible. This is of course one of the major issues in quantum chaos. (In some limited cases such an approximate connection is possible, as we discuss below.)

Lacking a quantitative theory of the wavefunctions of chaotic geometries, one can only analyze the observed wavefunctions for general trends. The influence of symmetries is evident from the displayed figures. The other important guide that can be used is to consider the influence of the semiclassical ray or particle dynamics on the wavefunctions.

One of the remarkable realizations that has been made recently is the recognition of the importance of classical periodic orbits (PO) to the quantum or wave mechanics. The discovery by Heller[3] that wavefunctions of chaotic geometries can often be "scarred" along periodic orbits has played a central role in analyzing wavefunctions. Some of the shorter PO of the Sinai billiard are shown in Fig. 7. In the case of the Sinai billiard, the PO can be divided into two major types: those which avoid the central disc and only hit the rectangle, and those which also hit the disc. The former are nonisolated, since there exist nearby trajectories which have the same character. In contrast, PO which hit the central disc are unstable and isolated, since nearby trajectories are not periodic. Both these types of PO are seen to play a role in the wavefunctions, as discussed below.

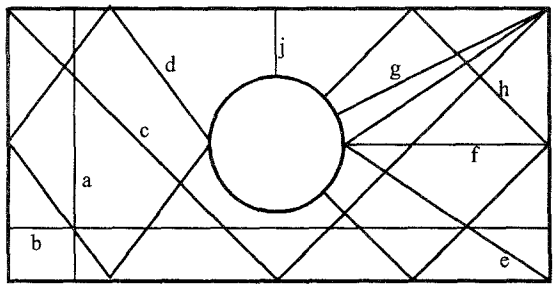

Fig. 7. Some of the periodic orbits of the Sinai billiard which are observed in the wavefunctions displayed in Fig. 6.

5.2.1. Nonisolated PO. Wavefunctions which can be associated with PO which only impinge on the outer rectangle are easily recognizable, since they retain the character of the wavefunctions of the bare rectangle. Besides the lowest four wavefunctions, a particularly striking example is the 4.028-GHz eigenstate. Here the presence of the disc appears to be entirely ignored. This is because it is possible to fit two more maxima into the region occupied by the disc. Families of these "rectangular" states can be seen, with another example being at 3.212 GHz. Another family of "quasirectangular" states can be recognized, with members at 3.475 and 4.074 GHz. These states seem to be distortions of the rectangular wavefunctions due to the presence of the disc. The well-known "bouncing ball" states are easily recognizable at 2.866 and 3.529 GHz. (It should be noted that these bouncing ball states also appear to be scarred along the diamond-shaped orbit d shown in Fig. 7.)

One aspect of these wavefunctions is worth noting. It is possible to arrive at a reasonably good estimation of the eigenvalues corresponding to the above eigenfunctions using the quantization rules for an appropriately chosen rectangular area. For instance, one would use the bare rectangular area for the "rectangular" states, and the left and right regions only for the bouncing ball states. Examples of such estimations are given in ref. 4.

5.2.2. Scars Along Isolated or Unstable PO. The cavity experiments discussed here have enabled the direct observation of wavefunctions which are scarred along some of the unstable PO specific to the Sinai billiard. Among the eigenfunctions displayed in Fig. 6, the PO along which scars are observed and the corresponding eigenvalues (the labels are from Fig. 7) are (d) 2.866 GHz, (e) 2.695 and 4.342 GHz, (f) 3.225 GHz, (g) 3.663 GHz, (h) 2.446 and 3.499 GHz, and (j) 2.913 GHz. We also note that the scar associated with the PO labeled c is observed in the 3.112-GHz state. Although this PO is really nonisolated, its presence is peculiar to the Sinai billiard.

The identification of scars and associated PO is unfortunately not enough to permit an estimation of the corresponding eigenvalue. Simple quantization along a single PO is inadequate, since the problem is inherently 2D and cannot be reduced to 1D. It will also be noticed that a given wavefunction may be scarred along more than a single PO. An example is the 3.499-GHz state, which is scarred along the POs c and h. This is more evident at higher frequencies, where multiple scars may be observed in a single wavefunction.

It is also apparent that there are many wavefunctions where scars cannot be clearly identified. (For example, the states at 3.767 GHz appear to reflect the circular symmetry of the central disc.) This may be due to the

greater instability of the PO in the Sinai billiard, in contrast, say, to the Bunimovich stadium, where apparently a substantial fraction of the wavefunctions are scarred. However, this may also be due to the difficulty of relying only on visual inspection to identify scars, which becomes increasingly difficult when the PO involve multiple bounces, or when more than one PO may be involved. Clearly a more quantitative approach is needed which does not rely on visual identification alone, and which may also enable a match to the corresponding eigenvalues. Some progress in "quantizing chaos" has been made using trace formulas for the eigenvalues, and it remains to be seen whether comparable success can be achieved for the eigenfunctions.

6. CONCLUSIONS AND SUMMARY

The discussion presented in this paper describes the utility of electromagnetic experiments studying wave or quantum chaos. Such experiments provide a well-controlled means of addressing important issues regarding the eigenvalues and eigenfunctions in closed geometries. The experiments are particularly powerful in providing direct physical realization of the wavefunctions, in contrast to other (atomic or nuclear) phenomena, where the principal observables are usually the eigenvalues and their statistics, while details of wavefunctions have indirect consequences[8] on phenomena such as scattering or ionization. The electromagnetic experiments have provided the first direct observation[4] of scars proposed earlier[3] on theoretical grounds, and underscore the importance of classical periodic orbits in the wave or quantum mechanics of classically chaotic systems. The results obtained here can be easily scaled down to atomic systems. For example, the Sinai billiard geometry studied here is relevant[9] to the helium atom.

Several other developments arising from such experiments are briefly mentioned here, and are the subject of future work. A more complete examination of the statistics of the eigenvalues and the wavefunctions is presently underway. We have also carried out a comparison[10] with numerical simulations, and found excellent agreement both as regards the eigenfunctions and the eigenvalue magnitudes. As noted earlier, the association of wavefunctions with PO is at the moment based upon visual suggestion, and is far from quantitative. It remains to be seen whether quantitative rules can be devised, as have recently been proposed in terms of trace formulas for the eigenvalues.[11]

The ability to easily vary parameters of the geometry and to study the parameter dependence of the wave dynamics is one of the powerful features of the experimental approach. For instance, the Sinai billiard is extremely

sensitive to small changes in the geometry, and such changes can be easily studied.[4] We have found that small changes in the disc location can lead to the phenomenon of quantum localization,[4,10] in which the waves are localized, even though the classical trajectories access all of the available space. In the experiment it is easy to vary the disc location. Some consequences of placing the disc in one corner have been presented earlier,[4] and a more complete study is ongoing.

Electromagnetic experiments of the type discussed here can also be used to study chaotic scattering in open geometries, as recent work has shown.[12] Extensions to 3D and the study of wave-packet dynamics are also feasible, although it must be noted that then the Maxwell and Schrödinger descriptions would be different.

The present situation in quantum chaos is reminiscent of an analogous period in classical particle chaos, before the discovery of general rules such as, for example, period-doubling bifurcations. There, too, analog experiments played an important role in elucidating phenomena, and the experiments discussed here may be viewed in a similar context.

ACKNOWLEDGMENTS

This work was supported by NSF-ECS-SGER-9114815, and the RSDF at Northeastern University.

REFERENCES

1. M. Berry, *Proc. Soc. Lond. A* **413**:182 (1987).
2. D. Kleppner, *Phys. Today* **44**:9 (1991).
3. E. J. Heller, *Phys. Rev. Lett.* **53**:1515 (1984).
4. S. Sridhar, *Phys. Rev. Lett.* **67**:785 (1991).
5. S. Sridhar and W. Kennedy, *Rev. Sci. Instr.* **59**:531 (1988); W. Kennedy, C. Zahopoulos, and S. Sridhar, *Solid State Commun.* **70**:741 (1989).
6. L. C. Maier and J. C. Slater, *J. Appl. Phys.* **23**:68 (1954).
7. H. Haake *et al.*, *Phys. Rev. A* **44**:6161 (1991); H. J. Stockman and J. Stein, *Phys. Rev. Lett.* **64**:2215 (1990).
8. R. V. Jensen *et al.*, *Phys. Rev. Lett.* **63**:2771 (1989).
9. R. V. Jensen, *Nature* **355**:591 (1992).
10. S. Sridhar and E. J. Heller, to be published.
11. M. V. Berry and J. Keating, *J. Phys. A* **23**:4839 (1990); M. Siebert and F. Steiner, *Phys. Rev. Lett.* **67**:1941 (1991).
12. E. Doron, U. Smilansky, and A. Frenkel, *Phys. Rev. Lett.* **65**:3072 (1991).